

Ultrasensitive resonance laser photoionization spectroscopy of the radioisotope chain¹⁵⁷⁻¹⁷² Tm produced by a proton accelerator

V. I. Mishin, S. K. Sekatskiĭ, V. N. Fedoseev, N. B. Buyanov,
V. S. Letokhov, G. D. Alkhazov,¹⁾ A. E. Barzakh,¹⁾
V. P. Denisov,¹⁾ V. S. Ivanov,¹⁾ and I. Ya. Chubukov¹⁾

*B. P. Konstantinov Leningrad Institute of Nuclear Physics, Academy of Sciences of the USSR, Gatchina and
Institute of Spectroscopy, Academy of Sciences of the USSR, Moscow*

(Submitted 27 January 1987)

Zh. Eksp. Teor. Fiz. **93**, 410-423 (August 1987)

A study was carried out of the hyperfine structure and isotopic shift of the 597.1 and 589.6 nm atomic lines of the radioisotopes¹⁵⁷⁻¹⁷² Tm. The measurements were performed by resonance laser photoionization of atoms in an atomic beam in line with a proton synchrocyclotron. The magnetic dipole and electric quadrupole moments and the mean square charge radii of nuclei were determined. A gradual reduction in the deformation of these nuclei with decreasing neutron number N was found. An irregularity was observed in the dependence of the mean square radius on N at $N = 94$. It was not present in the neighboring even- Z nuclei.

1. INTRODUCTION

Measurements of the magnetic dipole and electric quadrupole moments μ and Q and the mean square charge radii $\langle r^2 \rangle$ of nuclei belonging to long chains of radioisotopes (up to 20-30 isotopes), extending up to the limits of proton and neutron stability have recently become possible because of the high sensitivity and high resolution of laser spectroscopic techniques.¹⁻³ The information obtained by studying the properties of long chains of isotopes has substantially extended our ideas on the ground-state structure of the atomic nucleus. The spins and magnetic moments reflect the structure of the nuclear Fermi surface, the quadrupole moments measure the static deformation, and the mean square radii the deformation and zero-point oscillations of nuclei. Nuclear parameters deduced from optical data thus tell us, first, both about single-particle and collective properties of nuclei and, second, about both static and dynamic nuclear characteristics.

A "two-dimensional chart" of nuclear parameters covering a wide range of neutron and proton numbers, N and Z , is now evolving in the region corresponding to the rare-earth elements.

Isotope chains of the rare-earth elements Eu (Refs. 4-6), Gd, Dy, Er, and Yb (Refs. 7,8) have recently been investigated. It was established for even- Z elements that, with increasing distance from the magic proton number $Z = 64$ in a given isotope chain of a particular element, there is a change in the character of the transition from highly deformed to weakly deformed nuclei. For the samarium and gadolinium isotopes ($Z = 62, 64$), a sharp change in deformation is observed at $N = 88-90$. For the erbium and ytterbium isotopes ($Z = 68, 70$), there is no such discontinuity, i.e., the nuclear deformation of the isotopes of these elements varies gradually. For the dysprosium isotopes ($Z = 66$), there is an appreciable discontinuity, but its size is much smaller than that for the europium isotopes.

The nature of the transition region was not investigated for odd- Z nuclei. In the present paper, we report a study of odd- Z nuclei in this region, originally begun with a study of the europium isotopes.^{4,5} Preliminary data on the thulium isotopes were published in preprints.^{9,10}

The experiments were performed on the laser-nuclear complex at the Leningrad Institute of Nuclear Physics, using resonance layer photoionization of atoms, described in detail in Ref. 11. The detection sensitivity and spectral resolution were substantially improved as compared with the apparatus described in Ref. 12. The vacuum chamber containing the atomic beam source was mounted directly at exit from a mass separator, so that short-lived isotopes with half-lives up to a few tens of seconds could be investigated.⁴ In addition, use was made of an optical system allowing multiple crossing of the atomic beam by the laser beam. This resulted in an increase in the isotope detection sensitivity by more than an order of magnitude. A continuously-operating tunable single-frequency ring dye laser was used for the first excitation stage. This substantially increased the spectral resolution and enabled us to investigate the hyperfine structure of atomic lines and to obtain data on nuclear spins and moments.

The hyperfine structure and isotopic shifts were measured for two transitions, which made the final nuclear parameters more reliable.

2. PHOTOIONIZATION OF Tm

The method of stepwise laser photoionization of atoms was applied to the study of radioactive isotopes in Ref. 12, in which the radioisotopes of Eu were investigated. The optimum photoionization scheme chosen for thulium was based on the same considerations as those used for europium.

The first excitation stage consisted of transitions from the ground state $4f^{13}6s^2 \ ^2F_{7/2}^0$ to the two states $4f^{12}(^3H_6)5d_{5/2}6s^2(6,5/2)_{7/2}$ and $4f^{13}(^2F_{7/2}^0)6s6p(^3P_0^0)$. The wavelengths corresponding to these transitions, $\lambda_1 = 589.56$ and $\lambda_2 = 597.13$ nm, lie in the region of continuous generation of the rhodamine 6G dye laser.

The energy level scheme of thulium is relatively simple and many of its states have now been identified (Fig. 1).^{13,14} However, there are no published data that can be used to select the most efficient transitions for the second and third excitation stages. Autoionizing transitions from excited states have not been investigated, with the exception of Ref. 15. The oscillator strengths for transitions from the ground

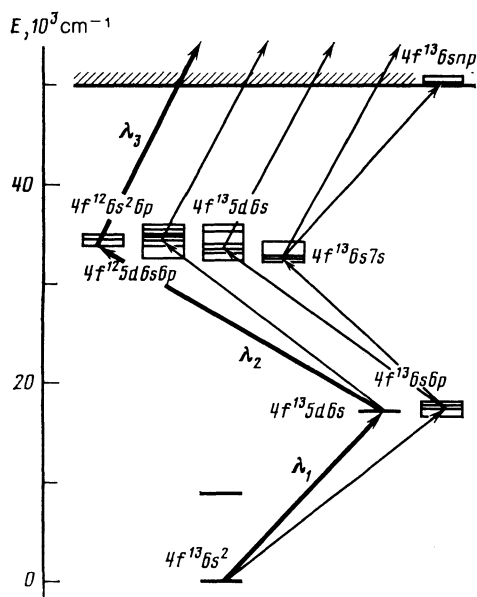


FIG. 1. Electron configurations and the transitions in the Tm atom that were employed ($\lambda_1 = 589.565$ nm, $\lambda_2 = 571.242$ nm, $\lambda_3 = 575.5$ nm).

and low-lying states have been measured in Refs. 16–18. No such data are available for transitions that could be used for the second and third excitation stages. We have therefore carried out an extensive study of wavelengths and cross sections corresponding to transitions from excited states to autoionizing states and have measured the cross sections for transitions between excited states.

The measurements were performed with the laser spectrometer described in Ref. 12. The relative efficiency of different three-stage photoionization schemes was determined for laser pulse energies below the saturation energy, using the formula

$$S_{\text{opt}} = KI v_1 v_2 v_3 / g_0 A_{01} \sigma_2 E_1 E_2 E_3, \quad (1)$$

where K is a constant, I is the amplitude of the photoion signal in relative units, v_i are the transition probabilities, g_0 is the statistical weight of the ground state, A_{01} is the probability of transition from the ground to the first excited state,^{16,19} E_i are the energies of the laser pulses, and σ_2 is the cross section for the second transition. The cross section σ_2 was determined from the excitation saturation curve, using the method described in Ref. 20. We examined about one hundred transitions to autoionizing states from different intermediate states. We selected only those transitions that resulted in the most efficient ionization of the thulium atoms by the radiation produced by dye lasers pumped by copper-vapor lasers. Table I lists the most effective transition se-

quences. Schemes Nos. 1 and 2 were used to investigate the radioactive isotopes.

3. APPARATUS

The radioisotopes were produced in a 14-g tantalum target, using spallation reactions initiated by 1-GeV protons accelerated in a synchrocyclotron. The separation of the isotopes according to their mass was performed by the mass separator of the IRIS complex. The 30-keV ions at exit from the mass separator were intercepted by a tantalum cylinder and were imbedded in the bottom of the cylinder (Fig. 2). The cylinder was used to convert ions to atoms. When the cylinder was heated to 1500 °C, the isotopes diffused out of the tantalum into the vacuum, and left the cylinder in the form of a collimated atomic beam propagating against the isotope beam from the mass separator. The length and diameter of the cylinder were 45 mm and 5 mm, respectively.

The atomic beam was crossed with the laser radiation at a distance of 54 mm from the edge of the cylinder. The laser beam was perpendicular to the atomic-beam axis in order to reduce Doppler broadening. Photoions produced as a result of the three-step photoionization of the isotopes were extracted by a constant electric field of 100 V/cm at right-angles to both the atomic and laser beams, and were detected by a secondary-electron channel multiplier. A set of metal diaphragms with alternately accelerating and retarding potential differences was placed between the cylinder and the interaction region, and was used to remove electrons and thermal ions and thus reduce the number of background ions reaching the photoionization region from the hot cylinder.

The photoionizing laser beam was formed from three beams with different frequencies tuned to resonance with the three successive transitions taking the atom to the autoionizing state. The photoion yield was increased by allowing the laser beam to cross the atomic beam several times, using two parallel mirrors. The effective number of transits of the laser beam through the atomic beam was 10–12. The width and height of the laser beam at entry to the multiple-transit optical system were 1 mm and 5 mm, respectively. This beam geometry was achieved by focusing the laser beam with a cylindrical lens (focal length 2 m). The beam diameter on the lens was 5 mm.

A Spectra Physics 380 continuously-operating single-frequency dye laser, pumped by the M2020 argon laser, was used to produce the first excitation stage in Tm. These are strong transitions, readily saturated by the continuous dye laser. Nevertheless, the radiation from the continuous dye laser was amplified by a pulsed dye laser pumped by pulses from a copper-vapor laser. This converted the continuous radiation into pulsed radiation, in which the pulse length and repetition frequency were determined by the corre-

TABLE I. The sequence of three quantum transitions resulting in the resonance ionization of the Tm atom from the ground state to the autoionizing state with energy E_a .

No.	λ_1 , nm	λ_2 , nm	σ_2 , 10^{-12} , cm ²	λ_3 , nm	S_{rel}	E_a , cm ⁻¹
1	589.565	571.242	1.1	575.5	1600	51 829
2	597.128	600.299	<0.6	552.4	>370	51 495
3	589.565	567.026	<0.6	584.4	>40	51 686
4	597.128	600.299	<0.6	551.8	>34	51 495

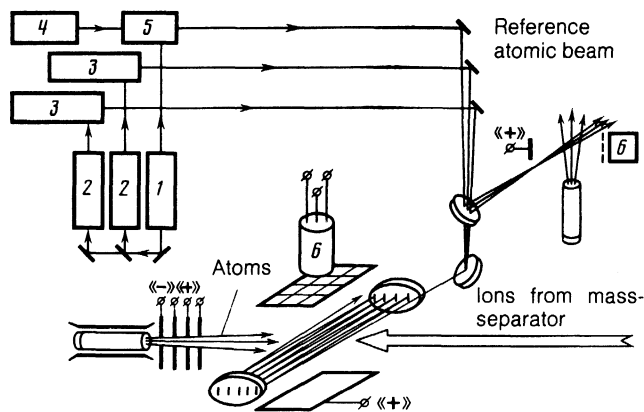


FIG. 2. Laser photoionization spectroscopy of radioisotopes: 1—copper-vapor laser; 2—copper-vapor amplifiers; 3—pulsed dye lasers; 4—single-frequency continuously operating dye laser; 5—pulsed dye laser; 6—secondary electron channel multipliers.

sponding parameters of the copper laser ($\tau_p \approx 16\text{--}18$ ns, $f = 10\,000$ s $^{-1}$). The amplification factor could be taken up to 10^4 or more. The power per amplified pulse was a few kW. The spectral width of the amplified radiation was largely determined by the pulse length, and was 20–30 MHz.

A pulsed laser is more convenient for the first excitation stage than a continuous laser for the following reasons. It is well-known that the instantaneous width of the spectrum generated by a single-mode dye laser is $\lesssim 1$ MHz. This means that, when this radiation interacts with the atomic beam, only a small fraction of atoms, equal to the ratio of the laser width to the Doppler width (in our case, 150 MHz), will be excited. On the other hand, when pulsed amplification is used, the spectral width is much greater and so the number of excited atoms is also greater.

The power per laser pulse is high enough to saturate the absorption throughout the Doppler-broadened line, which also increases the number of excited atoms. Thus, practically all the atoms undergoing the chosen transition in the atomic beam are excited. However, the spectral resolution is still determined by the Doppler width of the exciting line. In the absence of saturation, the intensities of the weak and strong hyperfine-structure components of the spin- $\frac{1}{2}$ Tm isotopes are approximately in the ratio of 1 to 20. This means that, when low-intensity beams of radioactive isotopes are employed, the weak components are practically undetectable. When saturation sets in, the intensity of the weak components becomes greater because it is then almost entirely determined by the population of the initial state and not by the excitation probability. In our experiments, the intensity ratio of the above components was 1:4, which significantly facilitated the interpretation of the spectra and the identification of the hyperfine-structure components.

Finally, pulsed radiation enables us to eliminate the phenomenon of optical pumping, which occurs when atoms with fine and hyperfine line structure are pumped by continuous radiation. The excitation of atoms by continuous radiation in the interval between ionizing laser pulses reduces the number of atoms in the initial state and, correspondingly, the number of atoms undergoing resonance ionization.

The transversely-pumped dye amplifier was assembled as follows. The amplifying cell through with the dye solution was passed (the cell design is the same as in the LZHI-504

laser²¹) was located at a distance of 6 m from the continuously-operating dye laser. The laser beam to be amplified was focused in the cell by a lens with a focal length of 1 m in such a way that the beam neck lay at the center of the cell. The copper-vapor laser beam was focused in the cell by a cylindrical lens with a focal length of 12 cm. The parameters of the amplifier were as follows. For a mean pump power of 2 W, the mean power of the amplified radiation and the continuous radiation between the pulses was 0.1 W. The superradiant power and the power carried by the continuous radiation between the pulses was 10–20 mW. The continuous-radiation output power sufficient to saturate the amplification was 10–50 mW. The spectral contrast, i.e., the ratio of amplified radiation power to the superradiant power in a spectral band equal to the bandwidth of the amplified radiation was at least 10^5 . The temporal contrast, i.e., the ratio of the mean power carried by the pulsed radiation to the continuous radiation power transmitted by the cell was greater than 10^4 .

For the second and third excitation stages, we used the LZHI-504 dye lasers,²¹ producing a spectral width of 25–30 GHz, which was definitely greater than the hyperfine width and the isotopic shift of the corresponding atomic transitions. All these lasers and the amplifier were pumped by three copper-vapor lasers, whose GL-202 active elements were supplied by three thyatron oscillators, gated simultaneously by a single electrical pulse through adjustable delay lines. One of the copper lasers was the master oscillator (Fig. 2). Its resonator consisted of a plane-parallel glass plate and a dielectric mirror with 50% reflectance. Radiation reflected by this mirror was directed into two copper-vapor amplifiers. The oscillators feeding these amplifiers were similar in design to those described in Ref. 22. The copper-vapor laser power on the side of the glass plate was 2 W and the power at exit of each amplifier was 6–8 W. The mean power produced by the pulsed dye lasers reached 0.8 W.

4. EXPERIMENTAL METHOD

The efficiency of detection by resonance photoionization, i.e., the ratio of the number of recorded photoions to the current of mass-separated ions when the radiation from all three dye lasers is tuned to resonance is largely determined by three factors. First, not all the atoms leaving the crucible reach the region of interaction with the laser radiation. The distance between the crucible and the laser beam is 54 mm. The size of the interaction region is 5×12 mm. When atoms escape from the crucible by effusion, the fraction of atoms reaching the interaction region should be determined by the geometric factor $\eta_{\text{geo}} = 0.001$. However, the long, hot cylinder collimates the beam of atoms leaving it, so that the fraction of atoms reaching the interaction region is actually $\eta_{\text{geo}} = 0.03$. The collimating properties of the cylinder were investigated by evaporating calibrated radioactive specimens onto a foil.²³ Second, some of the atoms cross the interaction region in the intervals between pulses. The fraction of illuminated atoms is determined by the transit factor $\eta_{\text{tr}} = mbf/v$, where m is the number of times where the laser beam crosses the atomic beam, b is the thickness of the laser beam along the atomic beam, v is the thermal velocity of the atoms, and f is the repetition frequency of the laser pulses. In our experiment, $\eta_{\text{tr}} = 0.2$. Finally, the photoion yield due to the three-stage photoionization in a single exposure to the

three pulses ($\lambda_1, \lambda_2, \lambda_3$) was $\eta_{ph} = 0.05$. This photoionization efficiency is determined, in the first instance, by the small cross section for the third transition to the autoionizing state ($\sigma_{aut} \approx 10^{-16} \text{ cm}^2$), which needs a dye laser producing 2–3 W for saturation, and this we did not have at our disposal. Thus, the total efficiency of detection of the Tm atoms implanted in the tantalum cylinder was $\eta = \eta_{geo} \times \eta_{tr} \times \eta_{ph} = 0.0003$.

The sensitivity of the system was determined both by the atom-detection efficiency and the background. Our apparatus suffers from a number of sources of background. First, there is the thermal-ion background due to surface ionization of different impurity elements in the atomic beam source. This background was suppressed by an electric screen placed in front of the photoionization region. At the temperature of the tantalum crucible (1500 °C), the thermal-ion background was less than 0.1 s^{-1} . Second, there is the radioactive background due to the decay of radioisotopes accumulated in the various components present in the vacuum chamber. The magnitude of this depends on the time at which the measurements are performed and on the radioactive properties of the isobars of the isotope under investigation. At worst, this background is less than 10 s^{-1} . Third, there is the background due to the ionization of the residual gas in the vacuum chamber by the high-energy ion beam from the mass separator. This background was suppressed for $10 \mu\text{s}$ before the appearance of the laser beam by cutting off the beam from the mass separator for $20 \mu\text{s}$. This time was sufficient for the ion cloud in the photoionization region between the extracting electrodes to spread out to a concentration at which the background was about 3 s^{-1} for a mass-separator beam current of about 10^7 s^{-1} . Under these conditions, the minimum isotope flux sufficient for measurements to be carried out was about 10^4 s^{-1} for a measurement time of about 2 h. This sensitivity was achieved for ^{138}Eu (Ref. 5) and ^{172}Tm .

The lifetimes of most of the isotopes examined were longer than the laser frequency scan time (1 min). We therefore employed the following device. The isotopes under investigation were accumulated in a cold crucible. The crucible was then rapidly heated, and the accumulated isotopes were evaporated in a few laser frequency scan cycles. The beam of mass-separated ions was cut off during this process. This procedure produced an improved signal-to-background ratio because the evaporation time could be made much shorter than the accumulation time. Moreover, in many cases, this method increased the quantity of the isotopes under investigation due to the decay of parent nuclei in the cold crucible. In the present case, these were the nuclei of ytterbium, for which the isotope flux corresponding to mass numbers $A = 160$ – 167 was much greater than the thulium flux with the same mass numbers. Moreover, in some cases, the accumulation and storage of the isotopes in the cold crucible enabled us to dispose of short-lived nuclear isomers, which was very important in the interpretation of the spectra because the hyperfine splitting of most of the thulium isotopes was small.

The isotopic shift of the atomic lines of the radioactive isotopes was measured against the stable reference isotope ^{169}Tm during the frequency scan of the laser used for the first excitation stage. A fraction of the radiation from the dye lasers was removed to a vacuum chamber isolated from the

mass separator, and a macroamount of the stable isotope was introduced into the atomic-beam source located in this chamber. To calibrate the frequency scale, we used a spherical interferometer with a baseline of 20 cm. Three spectra were thus produced when the continuous dye laser was frequency-scanned: The photoionization spectrum of the isotope under investigation, the photoionization spectrum of the stable isotope, and the transmission spectrum of the interferometer, consisting of equidistant lines used as frequency markers (Fig. 3). The separation between these markers was determined against the known position of hyperfine structure components of the stable isotope and was 371 MHz on average. The width of the frequency markers, determined by a convolution of the laser line profile and the instrumental line profile of the interferometer, was 50 MHz. The frequency of the dye laser used for the first excitation step was varied in the range 15–25 GHz in 1 min. The resolution of the spectral lines was determined by the residual Doppler broadening and by the degree of saturation of the first transition. It was found to be 150–300 MHz.

In most cases, the resolution was sufficient to enable us to measure the isotopic shift and the hyperfine splitting. The precision of our measurements was lower than that in experiments using collinear laser excitation of the fluorescence from fast atoms.²⁴ However, the precision of the nuclear parameters (especially the mean square radius and the quadrupole moment) deduced from the experimental data is usually limited not by experimental uncertainties, but by uncertainties in atomic calculations or in calibration data used to determine the required parameters.²⁵

5. RESULTS OF MEASUREMENTS AND THEIR ANALYSIS

The spectra obtained in the above way were analyzed as follows. We first determined the center of gravity of all the lines observed in the hyperfine structure spectra of a given isotope. The least-squares method was applied to these data to calculate the hyperfine structure constants that determined the position of the hyperfine structure components. The position of the hyperfine structure component $\nu_{F_1} \rightarrow \nu_{F_2}$ corresponding to the transition from the level with total an-

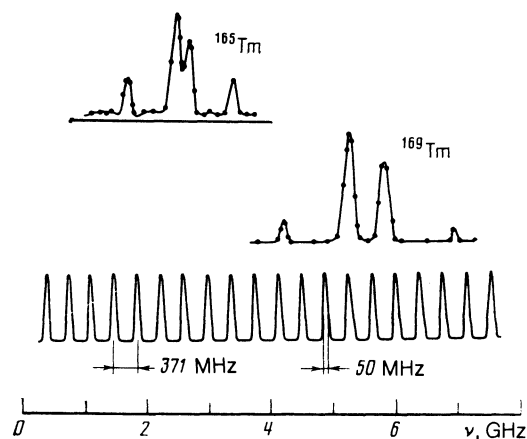


FIG. 3. Excitation spectra of the stable ^{169}Tm isotope and the radioactive ^{165}Tm isotope. The transmission bands of the spherical interferometer are shown under the spectra ($4f^{13}6s^{22}F_{7/2}^0 - 4f^{12}(^3H_6)5s_{5/2}6s^2(6,5/2)_{7/2}$; $\lambda = 589.565 \text{ nm}$).

TABLE II. Hyperfine structure constants and isotopic shifts of the initial state of Tm, calculated from the spectra recorded for the lines $\lambda^{(1)} = 597.13$ nm [$4f^{13}6s^2F_{7/2}^0-4f^{13}6s6p(7/2,0)_{7/2}$] and $\lambda^{(2)} = 589.56$ nm [$4f^{13}6s^2F_{7/2}^0-4f^{12}5d6s^2(6,5/2)_{7/2}$].

λ	I	$\lambda^{(1)}=597.13$ nm			$\lambda^{(2)}=589.56$ nm		
		a_i , MHz	b_i , MHz	Δv , MHz	a_i , MHz	b_i , MHz	Δv , MHz
157	1/2	760(20)	0	11 131(80)	778(30)	0	-13 220(60)
158	2	17(8)	-1009(200)	10 205(80)	14(12)	-950(250)	-12 080(100)
159	5/2	1103(7)	-2610(100)	8 650(35)	1105(10)	-2652(90)	-10 145(60)
160	1	123(10)	-813(60)	7 538(40)	138(20)	-760(80)	-8 790(40)
161	7/2	554(3)	-3960(100)	6 428(30)	557(5)	-3968(90)	-7 421(30)
162	1	54(6)	-940(50)	5 460(50)	56(7)	-934(40)	-6280(40)
163	1/2	{ -131(3)	0	4 101(20)	-130(5)	0	-
		{ -133,4(1,5) *	-	-	-	-	-3 993(40)
164	1	1919(15)	-972(70)	3 520(60)	1920(15)	-955(70)	-2 805(30)
165	1/2	{ -224(5)	0	2 534(20)	-225(5)	0	-4 570(40)
		{ -224,4(3,0) *	-	-	-	-	-
166	2	{ 36,6(3,0)	-2894(70)	2 128(30)	-	-	-2 380(10)
		{ 37,1(5) *	-	-	-	-	-
167	1/2	{ -318,5(8) *	-	-	-316(5)	0	-1 420(30)
168	3	61(3)	-4406(100)	855(40)	60(30)	-4400(400)	-1 050(10)
169	1/2	-374,14 *	0	0	-374,14 *	0	0
170	1	{ 195(13)	-1012(71)	-487(50)	-	-	-
		{ 200(3) *	-1010(15) *	-	-	-	-
171	1/2	{ -361(12)	0	-1 335(60)	-	-	1 360(10)
		{ -372(6) *	-	-	-	-	-
172	2	-	-	-	-	-	1 650(30)

Data from Ref. 26

gular momentum F_1 to the level with the total angular momentum F_2 is given by the well-known formula

$$W_{F_i} = a_i \frac{c_i}{2} + b_i \frac{\nu_{F_1 \rightarrow F_2} = \nu_0 + W_{F_2} - W_{F_1}, \quad {}^3/4 c_i (c_i + 1) - I(I+1) J_i (J_i + 1)}{2I(2I-1) J_i (2J_i - 1)}, \quad (2)$$

where

$$c_i = F_i(F_i + 1) - J_i(J_i + 1) - I(I + 1), \quad F_i = I + J_i, \quad i = 1, 2,$$

J_i is the total angular momentum of the electron shell of the atom in the ground ($i = 1$) and excited ($i = 2$) states, I is the nuclear spin, a_i and b_i are the magnetic and quadrupole hyperfine splitting constants, and ν_0 is the frequency of the unsplit transition. The measured nuclear spins of all the isotopes under investigation are reported in Refs. 26 and 27.

When the quantities ν_0 , a_1 , a_2 , b_1 , b_2 defining the position of the lines were determined, the ratio a_2/a_1 for the 589.56-nm line was fixed in accordance with the known magnetic splitting constants of the stable isotope ^{169}Tm (Ref. 26 and 28). Since, in this transition, the configurations have no unpaired $s_{1/2}$ and $p_{1/2}$ electrons, the hyperfine structure anomaly is small, i.e., a_2/a_1 is constant for all the isotopes. For example, in dysprosium, the hyperfine structure anomaly for a transition of this type is less than 0.017% of a_2/a_1 (Ref. 29).

The constants b_1 and b_2 were determined separately from the spectra of isotopes with well-resolved hyperfine structure. For the 589.56-nm transition, the ratio of these constants, found by analyzing the spectra of the isotopes $^{159,161}\text{Tm}$ is $b_2/b_1 = 0.51(2)$. For the 597.13-nm transition, this ratio was determined from the spectra of the isotopes $^{161,159,162,166}\text{Tm}$ and was found to be $b_2/b_1 = 0.79(4)$. The value of a_1 for ^{169}Tm (Ref. 26) was used to calibrate the frequency scale.

Table II lists the values of a_1 , b_1 , and $\Delta\nu$ for the 597.13 and 589.56 nm lines of the isotopes $^{157-172}\text{Tm}$. Our data are in good agreement with the values of a_1 and b_1 measured in Ref. 26 for some of the isotopes. For ^{172}Tm , the intensity of the weak hyperfine-structure components was so low that we were able to determine only the isotopic shift.

6. CHARGE RADII AND MOMENTS

The isotopic shift $\Delta\nu^{AA'}$ of an optical line accompanying the transition from an isotope with mass number A to an isotope with mass number A' is related to the change $\Delta\langle r^2 \rangle^{AA'}$ in the mean square charge radius by the formula²⁵

$$\Delta\nu^{AA'} = \Delta\nu_F^{AA'} + \Delta\nu_M^{AA'} = F\Delta\langle r^2 \rangle^{AA'} + M \frac{A' - A}{AA'}, \quad (3)$$

where $\Delta\nu_F$ and $\Delta\nu_M$ are, respectively, the field and mass shifts and F , M are constants depending on the structure of the wave functions.

These constants can be determined relatively readily for s - p transitions, using standard semiempirical formulas.²⁵ The 597.13-nm transition belongs to this type. The electron factor F is given by

$$F = E_{6s} \gamma f(Z) \quad (4)$$

where $E_{6s} = (\pi a_0^3 / Z) |\psi_{6s}(0)|^2$ was calculated by two gen-

erally adopted semiempirical methods, using the Goudsmit-Fermi-Segre formulas method (GFS method) and the data on the magnetic hyperfine structure constant of the valence s -electron (HFS method). In the GFS method we used the data from Ref. 30 and in the HFS method the data from Ref. 31. The average value was $E_{6s} = 0.421$. The screening factor γ was calculated by the Hartree-Fock method. According to Ref. 32, $\gamma = -0.73$. The factor $f(Z)$ was usually determined from the tables compiled by Babushkin.³³ However, the values for thulium are not present in these tables and we therefore used an interpolation because the dependence of f on Z was quite smooth. In accordance with Ref. 34, we included the factor $(n/N)^3$, where n is the principal quantum number in the nonrelativistic approximation and N is the relativistic "principal quantum number." Taking this factor into account, we found that $f(69) = 33.5 \text{ GHz/fm}^2$. The electron factor F for this transition is $F = -10.3 \text{ GHz/fm}^2$. The uncertainty in F is about 5%. The specific mass shift was assumed equal to zero.

The other transition used for the first stage of excitation is an f - d -transition (589.56 nm) for which the values of F and M were calculated with lower precision than those for the s - p -transition. Data obtained for the 589.56-nm transition were used to monitor the validity of the measured isotopic shifts on the King graph. It follows from (3) that the reduced isotopic shifts

$$\xi_i = \Delta\nu_i^{A,169} \left(\frac{A \cdot 169}{169 - A} \right) \left(\frac{169 - 167}{169 \cdot 167} \right) \quad (5)$$

for the two optical lines are linearly related. The constants in this linear expression were determined by the least-squares method: $\xi_2 = \alpha \xi_1 + \beta$, where $\alpha = -1.404(27)$, $\beta = 381(42) \text{ MHz}$. It is clear from Fig. 4 that the agreement between the isotopic shifts obtained for the two lines is good.

Table III lists the changes in the mean square radius, calculated from the known constants F and M . The uncertainties indicated in the table are experimental. The experimental values of ξ_i and the corresponding calculated values (straight line) are shown in Fig. 4. It is important to note that there is good agreement between the experimental and calculated values, which suggests that the approach used to calculate the atomic parameters for the f - d -transition was correct.

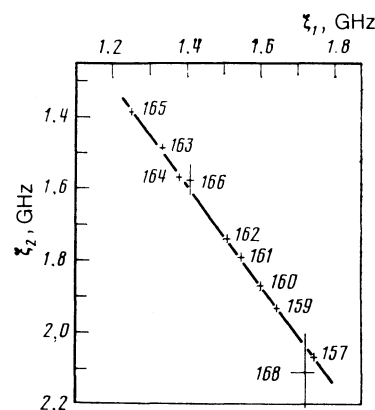


FIG. 4. King graph for the Tm lines. 597.13-nm line: $\xi_1, \text{GHz} = \Delta\nu_1^{A,169} (A \cdot 169 / 169 - A) (169 - 167 / 169 \cdot 167)$. 589.56-nm lines: $\xi_2, \text{GHz} = \Delta\nu_2^{A,169} (A \cdot 169 / 169 - A) (169 - 167 / 169 \cdot 167)$.

TABLE III. Change in the mean square charge radii of nuclei, magnetic moments, and electric quadrupole moments (spectroscopic and internal calculated from them) for the isotopes $^{157-172}\text{Tm}$.

A	$\Delta \langle r^2 \rangle_A, 10^6, \text{fm}^2$	$\mu, \text{n.m.}$	Q_s, barn	Q_0, barn
157	-1.093 (8)	0.475 (15)	0	-
158	-1.002 (8)	0.042 (20)	0.74 (15)	2.6 (5)
159	-0.850 (4)	3.41 (3)	1.93 (7)	5.4 (2)
160	-0.741 (4)	0.156 (18)	0.58 (4)	5.8 (4)
161	-0.632 (3)	2.39 (2)	2.90 (7)	6.2 (2)
162	-0.537 (5)	0.068 (8)	0.69 (3)	6.9 (3)
163	-0.404 (2)	0.082 (1)	0	-
164	-0.347 (6)	2.37 (2)	0.71 (5)	7.1 (5)
165	-0.250 (2)	0.139 (2)	0	-
166	-0.209 (3)	0.092 (1)	2.14 (3)	7.5 (1)
167	-0.126 (4)	0.197 (2)	0	-
168	-0.084 (4)	0.226 (11)	3.23 (7)	7.75 (18)
169	0	0.231 (2)	0	7.46 (16) [38]
170	0.048 (5)	0.247 (4)	0.74 (2)	7.4 (2)
171	0.131 (6)	0.230 (4)	0	-
172	0.154 (30)	<0.8	-	-

The most important result that follows from Fig. 4 is that the measured values of the isotopic shifts are correct.

The constants a and b are proportional to the magnetic dipole and spectroscopic quadrupole moments of the nucleus (μ and Q_s):

$$a = -\mu H(0)/II, \quad b = -e^2 Q_s \langle V_{zz}(0) \rangle (1-R)^{-1}, \quad (6)$$

where $H(0)$ and $V_{zz}(0)$ are, respectively, the magnetic field and electric-field gradient produced by the electron shell at the nucleus, and R is the Sternheimer correction.

The magnetic moment of ^{169}Tm was measured independently by the atomic-beam method.²⁶ The nuclear magnetic moments of the other isotopes of thulium can therefore be calculated from the formula

$$\mu_A = (a_A I_A / a_{169} I_{169}) \mu_{169}. \quad (7)$$

In this calculation, we neglect the hyperfine structure anomaly, which is usually less than 0.3%. An analogous relation is valid for the quadrupole moments:

$$(Q_s)_A = (b_A / b_{A_0}) (Q_s)_{A_0}, \quad (8)$$

where b_A and $(Q_s)_A$ are the value of the constant b and of the quadrupole moment of the isotope under investigation, and b_{A_0} and $(Q_s)_{A_0}$ are the corresponding values for the reference isotope. Unfortunately, independent measurements of Q_s , using mesic atoms, have not been carried out for the thulium isotopes. As indicated in Ref. 35, theoretical estimates of the Sternheimer correction are not accurate. Its magnitude for the thulium atom was therefore determined using experimental data for the neighboring rare-earth elements and then, as in the case of the analysis of isotopic shifts, the results were adopted for thulium. The validity of this procedure is thus confirmed by the fact that, according to the theory of the Sternheimer effect, the correction R , is approximately constant for electrons in a given shell in different atoms.³⁶ Using the average value of R_{4f} for erbium^{26,35} and holmium,^{26,37} and the quantities b_1 and $\langle V_{zz}(0) \rangle$ for ^{170}Tm reported in Ref. 26, we found that $(Q_s)_{170} = 0.74(2)$. The values of μ and Q_s , calculated from (7) and (8), are listed in Table III. The internal quadrupole moments Q_0 were calculated from the spectroscopic moments Q_s , using the standard strong-binding model:

$$Q_0 = Q_s (I+1) (2I+3) / I (2I-1). \quad (9)$$

7. DISCUSSION OF RESULTS

Figure 5 shows the mean square radius as a function of the mass number. As in the case of the even- Z isotopes of Er and Yb (7), this turns out to be a gradual variation for the odd- Z element Tm. The discontinuity found for nuclei near the magic number $Z = 64$ (Sm, Eu, Dy, and Gd) is absent from this dependence when $N = 90$. Figure 6 shows the differences between the mean square radii of neighboring even-even isotopes of Er, Yb, Dy, Eu, and Tm. They are actually equal to the slope of the mean square charge as a function of N . For the odd- Z nuclei, this dependence is typically different from the dependence for the neighboring elements Yb and Er. For example, when $N = 94$, there is an irregularity in the behavior of the mean square charge as a function of the neutron number, and a break appears on the curve. This irregularity is correlated with the irregularity in the behavior of the spins and magnetic moments (Table III). Our measured magnetic moments indicate that there is an irregularity in the filling of the proton states when $N < 94$. We note that the possible uncertainty in the atomic constant has no effect on the overall form of the data shown in Figs. 5 and 6. It is clear from Table III that the internal quadrupole moment Q_0 and, consequently, the deformation of the nuclei of

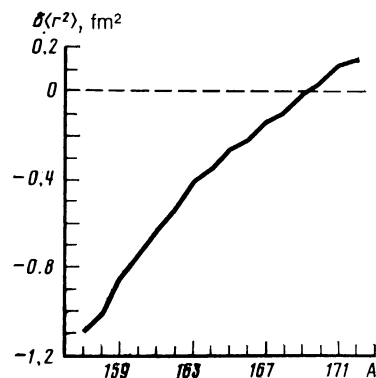


FIG. 5. Change in the mean square radius as a function of the atomic number for the thulium isotopes.

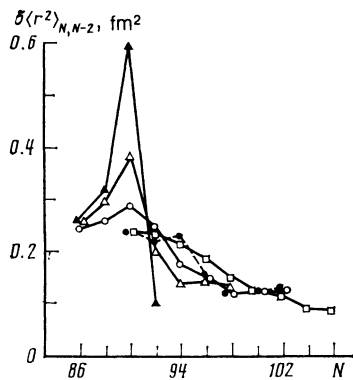


FIG. 6. Differential change in the mean square charge radius as a function of the number of neutrons in the even-even isotopes ^{66}Dy (∇), ^{68}Er (\circ), ^{70}Yb (\square) (Ref. 7) and the odd-odd isotopes ^{63}Eu (\blacktriangle) (Ref. 6) and ^{69}Tm (\bullet).

the Tm isotopes decreases quite smoothly with decreasing N , but the reduction is accelerated somewhat for $N < 94$.

The change in the mean square charge and the quadrupole moments of the Tm isotopes that we have investigated were calculated by the Hartree-Fock method with the effective Skyrme interaction and the macroscopic-microscopic approach. Good agreement was obtained with the quadrupole moment. A considerable discrepancy was noted between the description of the mean square radius as a function of N , obtained for $S3$ and SkM' . In contrast to $S3$, calculations with the SkM' forces provided a satisfactory description of this dependence for $N \geq 94$, and qualitatively reproduced the break found experimentally at $N = 94$. The discrepancy between theory and experiment for the "softer" nuclei ($N < 94$) is probably due to an increased contribution of zero-point oscillations that are not taken into account in either the Hartree-Fock or the macroscopic-microscopic theory. These nuclear parameters were also calculated by two other methods, namely, the liquid-drop model and the deformed Hartree-Fock method. The methodology and results are reported in detail in Refs. 10 and 39.

The nuclei ^{157}Tm and ^{158}Tm are of particular interest. The quadrupole moment Q_0 decreases sharply, between ^{159}Tm and ^{158}Tm and this should lead to a jump in $\Delta \langle r^2 \rangle$. However, this was not observed. This fact can be explained by assuming that the nuclei ^{157}Tm and ^{158}Tm are oblate or highly nonaxial. This interpretation of the experimental data is in agreement with the explanation of the nuclear spin of ^{157}Tm (equal to $\frac{1}{2}$) in terms of its nonaxial nature,⁹ and with the interpretation of the Tm isotopes in the transition region as nonaxial.⁴⁰

¹¹B. P. Konstantinov Leningrad Institute of Nuclear Physics, Academy of Sciences of the USSR, Gatchina

¹G. Huber, C. Thibault, R. Klapisch, *et al.*, *Phys. Rev. Lett.* **34**, 1209 (1975).

- ²T. K ue, P. Dabkiewicz, C. Duke, *et al.*, *Phys. Rev. Lett.* **39**, 180 (1977).
³G. D. Alkhazov, A. E. Barzakh, E. E. Berlovich, *et al.*, *Pis'ma Zh. Eksp. Teor. Fiz.* **37**, 231 (1983) [*JETP Lett.* **37**, 274 (1983)].
⁴G. D. Alkhazov, A. E. Barzakh, E. E. Berlovich, *et al.*, *Pis'ma Zh. Eksp. Teor. Fiz.* **40**, 95 (1984) [*JETP Lett.* **40**, 836 (1984)].
⁵V. N. Fedoseyev, V. S. Letokhov, V. I. Mishin, *et al.*, *Opt. Commun.* **52**, 24 (1984).
⁶S. A. Ahmad, W. Klempt, C. Ekstr m, *et al.*, *Z. Phys. A* **321**, 35 (1985).
⁷R. Neugart, *Lasers in Nuclear Physics*, ed. by C. E. Bemis and H. K. Carter, Nuclear Science Research Conference Series, Harwood Acad., Chur-London-Paris-New York, 1982, Vol. 3, p. 321.
⁸R. Neugart, K. Wendt, S. A. Ahmad, *et al.*, *Hyperfine Interactions*, 1983, Vol. 15/16, p. 181.
⁹A. E. Barzakh, V. P. Denisov, A. G. Deryatin, *et al.*, Preprint LIYaF AN SSSR No. 1079 [in Russian], 1985.
¹⁰G. D. Alkhazov, A. E. Barzakh, N. B. Buyanov, *et al.*, Preprint LIYaF AN SSSR No. 1145 [in Russian], 1985.
¹¹V. S. Letokhov, *Laser Photoionization Spectroscopy* [in Russian], Nauka, M., 1987.
¹²A. N. Zherekhin, O. N. Kompanets, V. S. Letokhov, *et al.*, *Zh. Eksp. Teor. Fiz.* **86**, 1249 (1984) [*Sov. Phys. JETP* **59**, 729 (1984)].
¹³J. Sugar, W. F. Meggers, and P. J. Camus, *J. Res. Nat. Bur. Stand. (USA)* **77**, 1 (1973).
¹⁴W. L. Martin, R. Zalubas, and L. Hagan, *Atomic Energy Levels. The Rare-Earth Elements*, NSRDS-NBS60, Washington, 1978.
¹⁵E. Vidolova-Angelova, G. I. Bekov, L. N. Ivanov, V. Fedoseev, and A. A. Atakhadjaev, *J. Phys. B Atom. Mol. Phys.* **17**, 953 (1984).
¹⁶C. Corliss and W. Bozman, *Transition Probabilities and Oscillator Strengths of 70 Elements* [Russ. Transl., Mir, Moscow, 1968].
¹⁷P. Camus, *J. Phys.* **31**, 985 (1970).
¹⁸K. B. Blagoev, V. A. Komarovskii, and N. P. Penkin, *Opt. Spektrosk.* **40**, 622 (1976) [*Opt. Spectrosc. (USSR)* **40**, 356 (1976)].
¹⁹V. A. Komarovskii and N. P. Penkin, *Opt. Spektrosk.* **26**, 882 (1969) [*Opt. Spectrosc. (USSR)* **26**, 483 (1969)].
²⁰R. V. Ambartsumyan, V. M. Apatin, V. S. Letokhov, *et al.*, *Zh. Eksp. Teor. Fiz.* **70**, 1660 (1976) [*Sov. Phys. JETP* **43**, 866 (1976)].
²¹V. I. Mishin, V. E. Mnushkin, V. G. Nikiforov, B. F. Trinchuk, and V. I. Fedorov, *Prib. Tekh. Eksp. No. 2*, 246 (1983).
²²V. V. Zubov, N. A. Lyabin, V. I. Mishin, *et al.*, *Kvantovaya Elektron. (Moscow)* **10**, 1908 (1983) [*Sov. J. Quantum Electron.* **13**, 1266 (1983)].
²³G. D. Alkhazov, A. E. Barzakh, E. E. Berlovich, *et al.*, Preprint LIYaF AN SSSR No. 908 [in Russian], 1983.
²⁴A. C. Mueller, F. Buchinger, W. Klempt, *et al.*, *Nucl. Phys. A* **403**, 234 (1983).
²⁵K. Heilig and A. Steudel, *Atom. Data Nucl. Data Tables* **14**, 613 (1974).
²⁶C. Ekstr m and I. L. Lamm, *Phys. Scr.* **7**, 31 (1973).
²⁷C. Ekstr m and L. Robertson, *Z. Phys. B* **A316**, 239 (1984).
²⁸W. J. Childs, L. S. Crosswhite, V. Pfeufer, *et al.*, *J. Opt. Soc. Am. B* **1**, 22 (1984).
²⁹D. Z. Clark, M. E. Cage, and G. W. Grenlees, *Phys. Lett. A* **62**, 439 (1977).
³⁰J. Sugar and J. Reader, *J. Opt. Soc. Am.* **55**, 1286 (1965).
³¹H. W. Brandt and P. Camus, *Z. Phys. B* **A283**, 309 (1977).
³²M. A. Coulthard, *J. Phys. B* **6**, 23 (1973).
³³F. A. Babushkin, *Zh. Eksp. Teor. Fiz.* **44**, 1661 (1963) [*Sov. Phys. JETP* **17**, 1118 (1963)].
³⁴D. Zimmermann, *Z. Phys. B* **A315**, 123 (1984).
³⁵Y. Tanaka, R. M. Steffen, I. B. Sherea, *et al.*, *Phys. Rev. C* **29**, 1830 (1984).
³⁶R. M. Sternheimer, *Phys. Rev.* **146**, 140 (1966).
³⁷R. J. Powers *et al.*, *Nucl. Phys. A* **262**, 493 (1976).
³⁸B. S. Dzhelepov, G. F. Dranitsyna, and V. M. Mikhailov, *Properties of Deformed Nuclei with $K = \frac{1}{2}$* [in Russian], Nauka, L., 1971, p. 251.
³⁹A. E. Barzakh and V. E. Starodubskii, Preprint LIYaF AN SSSR No. 1143 [in Russian], 1985.
⁴⁰R. Holzmann *et al.*, *Phys. Rev. C* **31**, 421 (1985).

Translated by S. Chomet